INTERNATIONAL JOURNAL FOR NUMERICAL METHODS IN FLUIDS
Int. J. Numer. Meth. Fluids 2002; **40**:903–925 (DOI: 10.1002/fld.381)

Zonal multi-domain RANS/LES simulations of turbulent flows

P. Quéméré[1] and P. Sagaut[2,*,†]

[1]*CEA Grenoble, DRN/DTP/SMTH/LDTA, 17 rue des Martyrs, 38054 Grenoble Cedex 9, France*
[2]*ONERA/DSNA, 29 av. de la Division Leclerc, 92 Châtillon, France*

SUMMARY

A new zonal multi-domain Reynolds averaged numerical simulation/large-Eddy simulation (RANS/LES) method is presented and assessed. The main occurring problem is the coupling at the domain interfaces between a 1D or 2D, ensemble averaged solution computed with the RANS approach with the 3D, filtered, unsteady solution obtained using the LES approach. Both low- and high-normal velocity interface cases are considered, resulting in a fully general approach. A coupling procedure well suited for cell-centred finite volume numerical method is proposed. Numerical tests are carried out for the plane channel and the plane plate with a blunt trailing-edge configurations. Copyright © 2002 John Wiley & Sons, Ltd.

KEY WORDS: RANS; LES; multidomain

1. INTRODUCTION

Direct numerical simulation of turbulent flows is still far out of range for flows of practical industrial interest. In order to get an unsteady high-frequency representation of the solution, large-Eddy simulation (LES) has been investigated by many authors (see Reference [1] for a review). This technique, which is based on a low-pass filtering of the exact solution of the Navier–Stokes equations, makes it possible to obtain a significant reduction in the complexity of the simulation by reducing the number of degrees of freedom. But LES is still subject to severe constraints when wall bounded flows are considered, because (at least theoretically) the internal region of the boundary layer needs to be quasi-directly resolved, yielding large computational costs.

Because an accurate unsteady description of the solution is not needed everywhere when dealing with practical engineering problems, the idea of using zonal approaches has emerged. The idea is here to use LES in small localized subdomains where an accurate description of the flow is wanted, while computing the rest of the configuration with a low-accuracy method. The later method will be the Reynolds averaged numerical simulation (RANS) approach in the present work.

*Correspondence to: P. Sagaut, ONERA, DSNA/ETRI, 29 av. de la Division Leclerc, 92320 Chatillon, France.
†E-mail: sagaut@onera.fr

Received 9 March 2001
Revised 12 April 2002

Previous authors have proposed hybrid RANS/LES approaches, but most of them are based on the definition of a universal turbulence model, which is able to switch from LES to RANS. Two recent examples are the detached Eddy simulation of Spalart [2] and the hybrid model of Speziale [3]. The former was recently shown to yield not fully satisfactory results for attached flows [4], while no results based on the later have been published up to now.

The approach proposed in the present paper is based on a multi-domain/multi-resolution decomposition of the problem. The full configuration is decomposed into several subdomains, which can be treated with either RANS or LES approach. The problem is now to define adequate interface conditions between RANS and LES subdomains. This problem is a fully general multi-domain problem, which is a generalization of the LES multi-resolution/multi-domain approach proposed by Quéméré *et al.* [5].

The paper is organized as follows. The theoretical framework associated to the problem is introduced in Section 2. Corresponding governing equations and physical models are discussed in Section 3. The RANS/LES interface problem and the proposed interface numerical treatment are detailed in Section 4. Section 5 presents the main features of the numerical method. Two test cases are then discussed: the subsonic plane channel flow (Section 6), and the flow past a blunt trailing edge (Section 7). Conclusions and perspectives are presented in Section 8.

2. STATEMENT OF THE SCALE-SEPARATION PROBLEM

Both RANS and LES approaches rely on a scale-separation procedure. In the former case, it is obtained via a statistical average, leading to

$$\phi(x,t) = \langle \phi(x,t) \rangle + \phi'(x,t) \tag{1}$$

where ϕ is a space- and time-dependent dummy variable, and $\langle . \rangle$ denotes the ensemble average operator defined as

$$\langle \phi(x,t) \rangle = \frac{1}{N} \sum_{i=1,N} \phi_i(x,t) \tag{2}$$

where N is the total number of independent samples ϕ_i considered to perform the ensemble average. Invoking the ergodic theorem, it is important to note that the dimension of the averaged problem is lower than the one of the original problem for a large class of flows: the original problem involves four dimensions (three for space, one for time), while the dimension of the averaged problem ranges from 0 to 4.

In the case of LES, scale separation is traditionally associated to the use of a spatial convolution filter, yielding

$$\phi(x,t) = \bar{\phi}(x,t) + \phi''(x,t) \tag{3}$$

with

$$\bar{\phi} = \int G(x-\xi;\Delta)\phi(\xi)\,\mathrm{d}\xi \tag{4}$$

where G is the kernel filter function and Δ is the cut-off lengthscale associated with the filter. For sake of simplicity we restrict ourself to a formal presentation, and the extension of the

convolution filter to the non-homogeneous case (see References [1, 6, 7]) will not be detailed here. It is important noting that all the developments presented below are fully general. The dimension of the filtered problem is the same as in the original problem: three dimensions for space and one dimension for time.

3. GOVERNING EQUATIONS AND CLOSURES

3.1. Governing equations for resolved motion

We consider here the case of Newtonian compressible fluids. The fluid motion and thermodynamic state is described by the compressible Navier–Stokes equations

$$\begin{aligned} \frac{\partial \rho}{\partial t} + \frac{\partial}{\partial x_j}(\rho u_j) &= 0 \\ \frac{\partial(\rho u_i)}{\partial t} + \frac{\partial}{\partial x_j}(\rho u_i u_j + p\delta_{ij} - \sigma_{ij}) &= 0, \quad i = 1,2,3 \\ \frac{\partial(\rho E)}{\partial t} + \frac{\partial}{\partial x_j}(\rho E u_j + p u_j - \sigma_{ij} u_i + q_j) &= 0 \end{aligned} \tag{5}$$

where u, p, and ρ are the velocity, the static pressure and the density, respectively. The gas is assumed to be perfect

$$p = \rho R T \tag{6}$$

where R is the perfect gas constant.

The total energy E, the viscous stress tensor σ and the heat flux q are expressed as

$$\begin{aligned} \sigma_{ij} &= -\frac{2}{3}\mu \frac{\partial u_j}{\partial x_j}\delta_{ij} + \mu\left(\frac{\partial u_i}{\partial x_j} + \frac{\partial u_j}{\partial x_i}\right) \\ \rho E &= \rho e + \frac{1}{2}\rho u_i u_i = \frac{p}{\gamma - 1} + \frac{1}{2}\rho u_i u_i \\ q_i &= -\kappa \frac{\partial T}{\partial x_i} \end{aligned} \tag{7}$$

where e is the internal energy and $\gamma = C_p/C_v$ is the ratio of the specific heat set equal to $\gamma = 1.4$. The molecular viscosity μ and conductivity κ are evaluated using the Sutherland law

$$\mu = \mu(T) = \mu_0 \sqrt{\frac{T}{T_0}} \frac{1 + C/T_0}{1 + C/T}$$

$$\kappa = \kappa(T) = \frac{\mu(T) C_p}{Pr}$$

where Pr is the number of Prandtl (set equal to 0.7), C_p the iso-pressure specific heat coefficient and T_0, μ_0 and C are values of reference depending on the gaz.

Applying one of the two-scale separation approaches described in the previous section (noted here by a bare) to the Navier–Stokes equations, we get the evolution equations for the resolved motion. These equations, which are *formally* equivalent, can be written as follows:

$$\frac{\partial \bar{\rho}}{\partial t} + \frac{\partial}{x_j}(\bar{\rho}\widetilde{u_j}) = 0 \tag{8}$$

$$\frac{\partial(\bar{\rho}\widetilde{u_i})}{\partial t} + \frac{\partial}{\partial x_j}(\bar{\rho}\widetilde{u_i}\widetilde{u_j} + \bar{p}\delta_{ij} - \widetilde{\sigma_{ij}}^*) = A_1 + A_2 \tag{9}$$

$$\frac{\partial(\bar{\rho}\tilde{E}^*)}{\partial t} + \frac{\partial}{\partial x_j}(\bar{\rho}\tilde{E}^*\widetilde{u_j} + \bar{p}\widetilde{u_j} - \widetilde{\sigma_{ij}}^*\widetilde{u_i} + \widetilde{q_j}^*) = B_1 + \cdots + B_7 \tag{10}$$

where the tilde symbol refers to mass-weighted variables

$$\tilde{\phi} = \frac{\overline{\rho\phi}}{\bar{\rho}} \tag{11}$$

The modified total energy $\bar{\rho}\tilde{E}^*$ is defined as

$$\bar{\rho}\tilde{E}^* = \bar{\rho}\tilde{e} + \frac{1}{2}\bar{\rho}\widetilde{u_i}\widetilde{u_i} = \frac{\bar{p}}{\gamma - 1} + \frac{1}{2}\bar{\rho}\widetilde{u_i}\widetilde{u_i} \tag{12}$$

and the modified viscous stress tensor $\widetilde{\sigma_{ij}}^*$ and the modified heat flux $\widetilde{q_i}^*$ as

$$\overline{\sigma_{ij}}^* = -\frac{2}{3}\mu(\tilde{T})\frac{\partial \widetilde{u_j}}{\partial x_j}\delta_{ij} + \mu(\tilde{T})\left(\frac{\partial \widetilde{u_i}}{\partial x_j} + \frac{\partial \widetilde{u_j}}{\partial x_i}\right) \tag{13}$$

$$\overline{q_i}^* = -\kappa(\tilde{T})\frac{\partial \tilde{T}}{\partial x_i} \tag{14}$$

$$\tag{15}$$

The state law associated to these new variables is

$$\bar{p} = \bar{\rho}R\tilde{T} \tag{16}$$

The unresolved terms appearing in the momentum and energy equations are defined as follows:

$$A_1 = -\frac{\partial}{\partial x_j}\tilde{\rho}(\widetilde{u_i u_j} - \widetilde{u_i}\widetilde{u_j}) \tag{17}$$

$$A_2 = \frac{\partial}{\partial x_j}(\overline{\sigma_{ij}} - \widetilde{\sigma_{ij}}^*) \tag{18}$$

$$B_1 = \frac{\partial}{\partial x_j}(\overline{\rho e u_j} - \overline{\rho e}\,\widetilde{u_j}) \tag{19}$$

$$B_2 = \left(\overline{p \frac{\partial u_i}{x_i}} - \bar{p} \frac{\partial \widetilde{u_i}}{\partial x_i} \right) \tag{20}$$

$$B_3 = \frac{\partial}{\partial x_j} \bar{\rho}(\widetilde{u_i u_j} - \widetilde{u_i}\widetilde{u_j})\widetilde{u_i} \tag{21}$$

$$B_4 = \bar{\rho}(\widetilde{u_i u_j} - \widetilde{u_i}\widetilde{u_j}) \frac{\partial \widetilde{u_i}}{\partial x_j} \tag{22}$$

$$B_5 = \left(\overline{\sigma_{ij} \frac{\partial u_j}{\partial x_i}} - \overline{\sigma_{ij}} \frac{\partial \widetilde{u_j}}{\partial x_i} \right) \tag{23}$$

$$B_6 = \frac{\partial}{\partial x_j} (\overline{\sigma_{ij}}\widetilde{u_j} - \widetilde{\sigma_{ij}}^{*} \widetilde{u_j}) \tag{24}$$

$$B_7 = \frac{\partial}{\partial x_j} (\overline{q_j} - \widetilde{q_j}^{*}) \tag{25}$$

The specific closures associated to LES and RANS approaches are described in the following sections.

3.2. LES closure

The subgrid models and underlying assumptions used in this study are the same than those employed by Lenormand *et al.* [8, 9] for subsonic and supersonic flows. This approach relies on the previous works of Vreman [10]. Since there is nothing new dealing with that point, we only briefly recall the main features of the models.

Following Vreman's conclusions [10], the A_2, B_5, B_6 and B_7 can be neglected. Considering subgrid-viscosity-type models relying on the Boussinesq hypothesis, we get

$$\begin{aligned} A_1 &= \frac{\partial \tilde{\tau}_{ij}^{\mathrm{L}}}{\partial x_j} \\ B_3 &= \frac{\partial \tilde{\tau}_{ij}^{\mathrm{L}} \tilde{u}_i}{\partial x_j} \\ B_4 &= \tilde{\tau}_{ij}^{\mathrm{L}} \frac{\partial \widetilde{u_i}}{\partial x_j} \\ B_1 + B_2 &= -\frac{\partial}{\partial x_j} \left(\frac{\mu_{\mathrm{t}}^{\mathrm{L}} C_p}{Pr_{\mathrm{t}}} \frac{\partial \tilde{T}}{\partial x_j} \right) \end{aligned} \tag{26}$$

where the subgrid Prandtl number Pr_{t} is set equal to 0.6 and where the deviatoric part $\tilde{\tau}_{ij}^{\mathrm{L,D}}$ of the subgrid-scale stress tensor $\tilde{\tau}_{ij}^{\mathrm{L}} = \bar{\rho}(\widetilde{u_i u_j} - \widetilde{u_i}\tilde{u_j})$ (with superscript L referring to as LES approach) is modelled by

$$\tilde{\tau}_{ij}^{\mathrm{L,D}} = \tilde{\tau}_{ij}^{\mathrm{L}} - \frac{1}{3} \tilde{\tau}_{kk}^{\mathrm{L}} \delta_{ij} = -\mu_{\mathrm{t}}^{\mathrm{L}} \left(\frac{\partial \widetilde{u_i}}{\partial x_j} + \frac{\partial \widetilde{u_j}}{\partial x_i} \right) \tag{27}$$

The subgrid-scale viscosity μ_t^L is computed using the Selective Mixed-Scale Model [1, 8, 9, 11]. This model is given by a non-linear combination of the norm of the vorticity $\tilde{\omega}$, the characteristic length scale Δ and the kinetic energy $\widetilde{q_c}^{1/2}$ of the highest resolved frequencies

$$\widetilde{\mu}_t = C_m f_{\theta_0}(\theta)\bar{\rho}|\tilde{\omega}|^{1/2}\Delta^{3/2}\widetilde{q_c}^{1/2} \tag{28}$$

with $C_m = 0.06$ and f_{θ_0} the selective function. Introducing a test filter denoted with a hat ($\widehat{\tilde{u}_i} = \tilde{u}_{i-1}/4 + \tilde{u}_i/2 + \tilde{u}_{i+1}/4$) which can be interpreted as a second-order approximation of a Gaussian filter [9], the kinetic energy q_c is evaluated by

$$\widetilde{q_c}^2 = \tfrac{1}{2}(\tilde{u}_i - \widehat{\tilde{u}}_i)(\tilde{u}_i - \widehat{\tilde{u}}_i)$$

3.3. RANS closure

As in the LES case, fluctuations of molecular viscosity and diffusivity are neglected. Only the terms A_1, B_3 and the contribution of terms $B_1 + B_2$ are taking into account (the effects of term B_4 are small in regard to the other ones for the applications aimed).

As for LES, the RANS closure employed in the present study is based on the definition of an Eddy-viscosity μ_t^R (superscript R referred to as RANS approach), yielding

$$\tilde{\tau}_{ij}^R = \bar{\rho}\widetilde{u_i'' u_j''} = \frac{2}{3}\mu_t^R \frac{\partial \widetilde{u_k}}{\partial x_k}\delta_{ij} - \mu_t^R\left(\frac{\partial \widetilde{u_i}}{\partial x_j} + \frac{\partial \widetilde{u_j}}{\partial x_i}\right) + \frac{2}{3}\rho k \delta_{ij} \tag{29}$$

where μ_t^R remains to be defined, and $k = \frac{1}{2}\widetilde{u_i'' u_i''}$ (with $u_i'' = u_i - \tilde{u}_i$) is the turbulent kinetic energy. Unlike the LES modelling, the later variable is explicitly taking into account in the RANS approach.

We use here the two-equation k–ε model [12]

$$\mu_t^R = C_\mu f_3 \frac{(\bar{\rho}k)^2}{\bar{\rho}\varepsilon} \tag{30}$$

where $C_\mu = 0.09$ is a constant, ε is the turbulent dissipation and f_3 a damping function to be defined below. The two turbulent quantities k and ε are computed by solving the following additional equations:

$$\frac{\partial(\bar{\rho}k)}{\partial t} + \frac{\partial(\bar{\rho}k\widetilde{u_i})}{\partial x_i} = -\bar{\rho}\widetilde{u_i'' u_j''}\frac{\partial(\widetilde{u_i})}{\partial x_j} - \frac{\partial}{\partial x_i}\left[\left(\mu + \frac{\mu_t^R}{\alpha_k}\right)\frac{\partial k}{\partial x_i}\right] - \bar{\rho}\varepsilon - 2\mu\left(\frac{\partial\sqrt{k}}{\partial x_i}\frac{\partial\sqrt{k}}{\partial x_i}\right) \tag{31}$$

$$\frac{\partial(\bar{\rho}\varepsilon)}{\partial t} + \frac{\partial\bar{\rho}\varepsilon\widetilde{u_i}}{\partial x_i} = -C_{\varepsilon_1} f_1 \frac{\varepsilon}{k}\bar{\rho}\widetilde{u_i'' u_j''}\frac{\partial(\widetilde{u_i})}{\partial x_j} - \frac{\partial}{\partial x_i}\left[\left(\mu + \frac{\mu_t^R}{\alpha_\varepsilon}\right)\frac{\partial\varepsilon}{\partial x_i}\right] - C_{\varepsilon_2} f_2 \bar{\rho}\frac{\varepsilon^2}{k} + 2\mu\mu_t^R\left(\frac{\partial^2\widetilde{u_i}}{\partial n_i^2}\right)^2 \tag{32}$$

with

$$\alpha_k = 1, \quad C_{\varepsilon_1} = 1.57, \quad C_{\varepsilon_2} = 2, \quad \alpha_\varepsilon = 1.3$$

and where n is the wall-normal unit vector and f_i the following damping functions:

$$f_1 = 1, \quad f_2 = [1 - 0.3\exp(-R_t^2)], \quad f_3 = \exp\left[\frac{-2.5}{\left(1 + \frac{R_t}{50}\right)}\right]$$

R_t is the turbulent Reynolds number, defined as $R_t = \bar{\rho}k/\mu\varepsilon$.

The turbulent heat flux appearing in the energy equation ($\partial\widetilde{q}_{t_j}/\partial x_j = B_1 + B_2$) is modelled using a first gradient hypothesis, similarly to LES closure, yielding

$$\tilde{q}_{t_j} = -\frac{\mu_t^R C_p}{Pr_t}\frac{\partial T}{\partial x_j} \tag{33}$$

where the turbulent Prandtl number Pr_t is taken equal to 0.9.

4. RANS/LES COUPLING AT THE SUBDOMAIN INTERFACE

4.1. Theoretical presentation of the problem

For sake of simplicity, and without loss of generality, the theoretical presentation of the problem is carried out in the case of the interface of two subdomains. A RANS simulation is carried out in the first one, referred to as Ω_1, while a LES simulation is performed in the second subdomain, Ω_2. The interface between the two subdomains is noted Γ_{12}. Data associated to the lth subdomain will be noted with the superscript (l).

The difference in the scale-separation operator selected in each subdomain leads to a discontinuity of the solution at the interface Γ_{12}

$$\bar{u}^{(1)}(x,t) \neq \bar{u}^{(2)}(x,t) \quad \text{on } \Gamma_{12} \tag{34}$$

preventing the use of classical conservative treatments of the interface. This can be seen as a generalization of the discontinuous interface condition derived for multi-domain/multi-resolution LES/LES simulations developed by Quéméré *et al.* [5]. This decomposition is also formally equivalent to the one introduced by Labourasse *et al.* [13] to handle the problem of the reconstruction of turbulent fluctuations around a RANS solution.

It is important noting that the interface treatment is intrinsically based on the numerical method used to solve the governing equations. We present below an interface condition adapted to the RANS/LES multi-domain problem within the framework of finite-volume, cell-centred numerical methods. In the present approach, boundary conditions for each subdomain are prescribed by defining the values of the unknowns in rows of ghost cells associated to each domain and overlapping the other one.

We now introduce the interface variable w_{12}, defined as the difference between the two fields on the interface

$$w_{12} = \bar{u}^{(2)}(x,t) - \bar{u}^{(1)}(x,t) \quad \text{on } \Gamma_{12} \tag{35}$$

The basic interface problem is the following:

- *Boundary conditions for the RANS subdomain*: evaluate $\bar{u}^{(1)}(x,t)$ from $\bar{u}^{(2)}(x,t)$ in the ghost cells, and find the values of turbulence-model related variables (k,ε). This corresponds to removing the interface variable w_{12} from the LES field $\bar{u}^{(2)}(x,t)$ in the RANS subdomain ghost cells. This will be symbolically noted as

$$\bar{u}^{(1)}(x,t) = R[\bar{u}^{(2)}(x,t)], \quad k = R_k[\bar{u}^{(2)}(x,t)], \quad \varepsilon = R_\varepsilon[\bar{u}^{(2)}(x,t)] \tag{36}$$

  where R will be referred to as the restriction operator.
- *Boundary conditions for the LES subdomain*: evaluate $\bar{u}^{(2)}(x,t)$ from $\bar{u}^{(1)}(x,t)$ in the ghost cells and define the subgrid-scale viscosity (μ_t^L). This is equivalent to the problem of computing w_{12} in these cells, and corresponds to the reconstruction of the high-frequency fluctuations at the interface. This will be noted

$$\bar{u}^{(2)}(x,t) = E[\bar{u}^{(1)}(x,t)] \quad \text{or} \quad w_{12} = E[\bar{u}^{(1)}(x,t), \bar{u}^{(2)}(x,t)], \quad \mu_t^L = E_{\mu_t}[\bar{u}^{(1)}(x,t)] \tag{37}$$

  where E will be called the enrichment operator.

4.2. Boundary conditions for the RANS subdomain

Values of $\bar{u}^{(1)}(x,t)$ in the ghost cells are easily obtained by applying the ensemble average operator to the LES field $\bar{u}^{(2)}(x,t)$, yielding

$$\bar{u}^{(1)}(x,t) = R[\bar{u}^{(2)}(x,t)] \equiv \langle \bar{u}^{(2)}(x,t) \rangle \quad \text{in ghost cells} \tag{38}$$

In practice, the ensemble average can be associated to (i) an ensemble average performed using several statistically equivalent simulations, as for Carati's ensemble-averaged LES [14, 15], (ii) an average over homogeneous space directions, (iii) an average in time, or any combinations of these three possibilities. The most general one is the first one, but it is also the most expensive. In the present paper, the second solution is used.

Evaluating k and ε is a more difficult task. Numerical experiments have shown that a direct reconstruction of these variables in the ghost cells using the LES field yields poor results because they are very sensitive to the restriction operator, the number of samples available to perform the ensemble average being generally to low to ensure a good evaluation of ε.

A robust and efficient method is to compute k and ε using Equations (31) and (32) with $\langle \bar{u}^{(2)}(x,t) \rangle$ quantities as a mean velocity field everywhere in the LES subdomain Ω_2. It is important noting that here k and ε have no feedback on the LES field $\bar{u}^{(2)}(x,t)$ in the interior of the Ω_2 subdomain, and can be seen as two-coupled passive scalars within this domain. This allows the definition of turbulent variables which account for memory effects and the structure of the field at the interface, with a weak dependency on the implementation of the ensemble average operator. A drawback of this boundary conditions for the turbulent variables is that the total turbulent kinetic energy, defined as the sum of the resolved and the modelled parts, is not continuous at the interface. The two reasons for that are: (i) a Dirichlet conditions is not used and (ii) the exact total turbulent kinetic energy is theoretically continuous at the interface, but the use of RANS and LES models do not ensure this conservation properties. It is worth noting the subgrid models used in this study belong to the functional type (see Reference [1] for a detailed discussion) and do not represent accurately the subgrid stresses and the subgrid kinetic energy.

4.3. *Boundary conditions for the LES subdomain*

It was said in Section 4.1 that the problem of the definition of the LES field in the ghost cells which overlap the RANS subdomains is equivalent to evaluating the interface variable in these cells. Because the ensemble average can be mathematically interpreted as a projector, information related to the fluctuations in this subdomain is lost and cannot be reconstructed from the RANS field $\bar{u}^{(1)}(x,t)$ alone.

The distinction will be made here between outflow and inflow subdomain interfaces.

Outflow interfaces: correspond to interfaces where the flow is directed from the LES subdomain toward the RANS subdomain. In this case, the quantity w_{12} is extrapolated from the LES subdomain in the following way:

1. Compute $\langle \bar{u}^{(2)}(x,t) \rangle$ in LES subdomain in rows of cells located just in front of the interface, using the same restriction operator as for the RANS subdomain interface condition.
2. Evaluate the interface variable w_{12} in these cells as follows:

$$w_{12} = \bar{u}^{(2)}(x,t) - \langle \bar{u}^{(2)}(x,t) \rangle \quad \text{in } \Omega_2$$

3. Extrapolate w_{12} in the ghost cells, yielding the extrapolated w_{12}^*. In the present work, a weighted first-order accurate extrapolation is used. In the one-dimensional case, it is written as follows:

$$w_{12}^* = w_{12}(x_0 + \tfrac{1}{2}\Delta x, t) = C_{\text{extra}} w_{12}(x_0 - \tfrac{1}{2}\Delta x, t) \tag{39}$$

where x_0 is the position of the interface, Δx the size of the cell in the direction normal to the interface and C_{extra} the weighting factor. Numerical experiments have shown that the use of a second-order accurate extrapolation yield numerical instabilities. The weighting factor is introduced to account for the variation of the resolved fluctuating kinetic energy. Two factors are responsible for this variation:

(a) The grid resolution variation between the last interior cell in Ω_2 and the ghost cells, which is associated to a cut-off lengthscale variation in the LES filter.
(b) The physical variation of the fluctuating energy profile associated to the fact that this quantity may evolve from one space location to another one. The difference between the location of the ghost cells and the interior cells must then be accounted for. It was taken into account by Nicoud *et al.* [16] on the basis of *a priori* knowledge of the velocity scaling in the incompressible channel flow.

This variation makes it necessary to rescale the variable w_{12}, in order to have the proper kinetic energy.

The second factor is essentially flow dependent, while the first one is mesh dependent. For the present simulation the value for C_{extra} has been defined empirically as the ratio of the characteristic lengthscales, evaluated from the volume V of the cells

$$C_{\text{extra}} = \frac{\Delta_{12}}{\Delta_\Omega} = \left(\frac{V_{12}}{V_\Omega} \right)^{1/3} \tag{40}$$

where subscripts 12 and Ω are related to the ghost cell and the first interior cell, respectively.

4. Reconstruct the total LES field in the ghost cells

$$\bar{u}^{(2)}(x,t) = \bar{u}^{(1)}(x,t) + w_{12}^{*} \quad \text{in ghost cells} \tag{41}$$

It is worth noting that the problem of the reconstruction of the subgrid-scale viscosity μ_t^L in the ghost cells is close to the one of the definition of hybrid RANS/LES problem. Speziale [3] proposed to rescale the RANS Eddy-viscosity by using the following relationships:

$$\tau_{ij}^{L} = [1 - \exp(-\beta\Delta/L_K)]^n \tau_{ij}^{R}$$

where L_K designates the Kolmogorov length scale and β and n are coefficients to be adjusted. This last formulae appears to be not well suited to deal with problems having different dimensions at the interface. In order to recover a 3D subgrid-scale viscosity for the LES subdomains we propose simply here to extrapolate the viscosity from the inner cells to the ghost cells.

Inflow interfaces: are the most difficult case, because the information is now convected from the RANS subdomain toward the LES subdomain. This problem is very similar to the problem of the definition of turbulent inflow conditions for LES. It is now recognized that the definition of rough boundary conditions, which do not account for the two-point and two-time correlations of turbulent fluctuations can have deleterious effects [17].

The distinction will be made here between the low- and high-normal velocity inflow interfaces. We define here low-normal velocity (resp. high-normal velocity) interfaces as interfaces for which the numerical advection lengthscale $L_c = u_n \Delta t$ (where Δt is the time step and $u_n = \bar{u}^{(1)} \cdot n$ the inflow-normal velocity component, n being the inward-normal vector) of the information across the interface is small (resp. high) with respect to the characteristic lengthscale L of turbulent fluctuations near the interface.

For low-normal velocity interfaces, the fluctuations remain strongly correlated in space, and w_{12} can be extrapolated from the LES subdomain. The numerical treatment is then exactly the same as for outflow interfaces.

For high-normal velocity interfaces, turbulent fluctuations will be decorrelated in space near the interface, and the extrapolation technique can no longer be used. Several ways to reconstruct w_{12} have been assessed in this study, relying on the use of analytical deterministic definitions of the fluctuations or based on a long-range extrapolation technique, similar to the rescaling technique of Lund [18] for turbulent inflow conditions. The best results, presented here, have been obtained by simulating a plane channel flow, independently of the present calculation. At each time step, the complement w_{12} is extracted, rescaled and used to define the inflow condition. This method, which is the most accurate one, induces the extra computational cost associated with the auxiliary LES computation. But is remains beneficial because the secondary computation is carried out on very simple time-developing flows, and the total cost remains much lower than those of full LES on the configuration. This point will be illustrated in Section 7.

5. NUMERICAL METHOD

The basic numerical method is exactly the same as the one described in References [5, 19, 20]. It is based on a second-order accurate finite volume, cell-centred discretization of the compressible Navier–Stokes equations. The skew-symmetric form and a centred non-dissipative

scheme are used for the convection term. Spatial derivatives (temperature gradients, velocity gradients) present in diffusive fluxes are computed using staggered cells to evaluate gradients in order to ensure the coupling between odd and even cells, preventing spurious wiggles. Time integration is performed using a third-order three-stage compact Runge–Kutta time-stepping scheme.

For plane channel flow computations, the same forcing term as in References [8, 9] is used.

6. APPLICATION TO THE PLANE CHANNEL FLOW

The multi-domain/multi-resolution technique has first been assessed on a subsonic plane channel flow. The interface has been taken parallel to the solid wall, corresponding to outflow or low-normal velocity boundary condition for the LES subdomain, and to inflow and outflow boundary for the RANS subdomain. It is then a relevant test case to validate the associated treatment based on the extrapolation of the fluctuation w_{12}.

6.1. Physical problem and computational parameters

The selected configuration is the isothermal-wall plane channel flow (Figure 1). Periodic boundary conditions are used in the streamwise (x) and spanwise (y) directions. For notational convenience, all bar and tilde symbols associated previously to the resolved variables in the equations are left out. The restriction operator R is defined as the ensemble average over homogeneous direction (x, y). Statistical moments of the solution are computed by performing a statistical average in time and over the same homogeneous directions.

The size of the computational domain (L_x, L_y and L_z in the streamwise, spanwise and wall-normal direction, respectively) was chosen such that the two-point correlations in the streamwise and spanwise directions would be essentially zero at the maximum separation (half the domain size).

In the present work, all the computations have been performed with CFL number equal to 0.95. This small value makes it possible to assume that the time-filtering effects due to the use of finite time steps will be masked by the implicit space-filtering operation. Uniform mesh spacing is used in homogeneous direction, while a stretched grid following an hyperbolic tangent law distribution is used in the wall-normal direction.

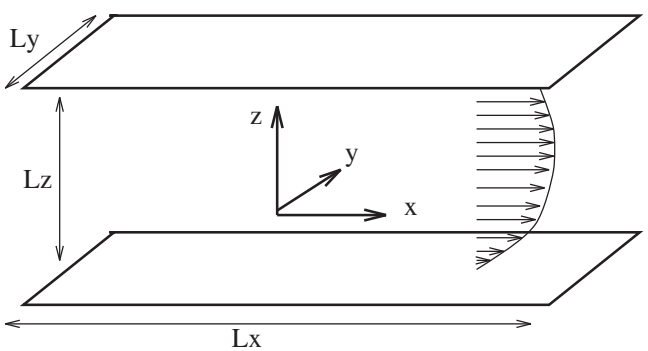

Figure 1. Plane channel configuration.

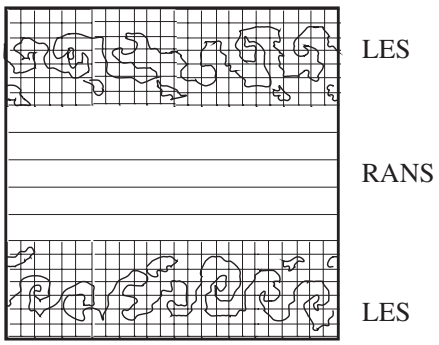

Figure 2. LES/RANS/LES configuration.

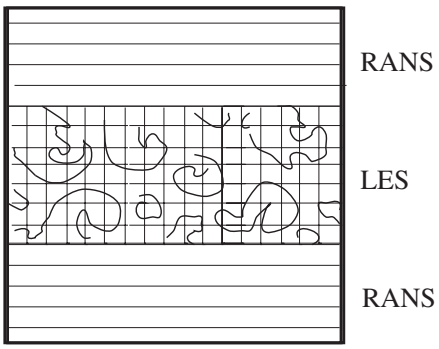

Figure 3. RANS/LES/RANS configuration.

Two configurations have been investigated:

- *Near-wall LES*: the internal boundary-layer region is resolved using LES, while the central part of the channel is described using RANS (Figure 2). That allows a fine description of the near-wall turbulent fluctuations, while ignoring the rest of the flow. This kind of description, which is required for some studies related to aeroacoustics and prediction of aero-optical effects, was the original purpose of the present work. For such applied studies, small LES subdomains embedded within a global RANS computations are used to get an accurate unsteady description of turbulent fluctuations in some near-wall regions.
- *Near-wall RANS*: the near-wall region is resolved using RANS, while the external boundary-layer region is resolved with LES (Figure 3). The RANS approach appears here like a wall model for LES. These computations can then be related to the DES approach [2, 4], or to the two-layer computations of Balaras *et al.* [21] and Cabot [22, 23].

6.2. Near-wall LES treatment

The tests presented in this section have been carried out using essentially a three-subdomain decomposition: one LES subdomain near each wall, and one RANS subdomain in the core

Table I. Computational parameters for monodomain reference RANS and LES simulations.

Case	Re_τ (target)	L_x	L_y	L_z	$N_x \times N_y \times N_z$	Δ_x^+	Δ_y^+	$\Delta_{z_w}^+ - \Delta_{z_c}^+$
A1L (LES)	590	2π	π	2	$55\times121\times129$	68	15	1–21
A1R (RANS)	590	—	—	2	$1\times1\times129$	—	—	1–21
B1L (LES)	1050	2.5π	$\pi/2$	2	$83\times83\times65$	100	20	1–50
B1R (RANS)	1050	—	—	2	$1\times1\times65$	—	—	1–50

Table II. Computational parameters for multi-domain RANS/LES simulations. The two or three values of N_z correspond to the number of grid point in the wall-normal direction in each subdomain.

Configuration	Case	Re_τ (target)	N_z	z_Γ^+	C_{extra}
LES/RANS	A2	590	65/65	590	1.000
LES/RANS/LES	A3	590	32/67/32	95	0.981
LES/RANS/LES	A3+	590	38/55/38	150	0.983
LES/RANS/LES	A3++	590	51/29/51	320	0.989
LES/RANS/LES	B3	1050	16/35/16	100	0.943
RANS/LES/RANS	A3RLR	590	38/55/38	150	0.95
RANS/LES/RANS	A3RLR+	590	45/41/45	225	0.95

region of the channel. Classical RANS and LES monodomain computations have also been performed in order to have some reference data.

Two targeted skin-friction Reynolds numbers have been considered: $Re_\tau = 590$ and $Re_\tau = 1050$, where Re_τ is defined as $Re_\tau = \sqrt{\rho_w Re(\partial\langle u\rangle/\partial z)_w}$. The Mach number M_0, defined from the bulk velocity u_b and the mean sound velocity at the wall as $M_0 = u_b/a_w$ is set equal to 0.5.

Computational parameters for all the simulations are presented in Tables I and II. The size of the domain is the same for the monodomain and the multi-domain computations at the same Reynolds number. For multi-domain simulations, z_Γ^+ is related to the distance between the wall and the interface, expressed in wall units. It is worth noting that in all cases the LES zone is large enough to capture the turbulent near-wall autonomous cycle [24, 25]. Thus, the production of turbulent fluctuations is ensured.

The computed mean values are summarized in Table III. A good agreement between reference monodomain and multi-domain computation is observed. It is seen that the friction Reynolds number is recovered within a 2% error level, which is a very satisfactory result. For the high-Reynolds number case, the multi-domain is seen to yields better results than the classical LES calculation.

Computed mean velocity profiles and resolved Reynolds stresses are compared with those obtained using an usual LES approach in Figures 4–7. The agreement obtained with the theoretical mean velocity profile is very satisfactory, and it is observed that the hybrid computations yield results which are very close to the LES results. The observed discrepancies at the highest Reynolds number are usual in LES computations with a second-order accurate

Table III. Computed mean values: friction Reynolds number Re_τ, friction velocity u_τ, centreline velocity U_c, centreline temperature T_c, wall density ρ_w.

Case	Re_τ	$u_\tau * 10^2$	U_c	T_c	ρ_w
A1L	593	5.20	1.10	1.045	1.044
A1R	595	5.23	1.13	1.039	1.040
A3	597	5.24	1.10	1.0445	1.042
A3+	604	5.30	1.095	1.045	1.044
A3++	590	5.17	1.10	1.045	1.044
B1L	986	4.45	1.010	1.051	1.05
B1R	1110	5.05	1.123	1.033	1.045
B3	1020	4.63	1.089	1.050	1.048

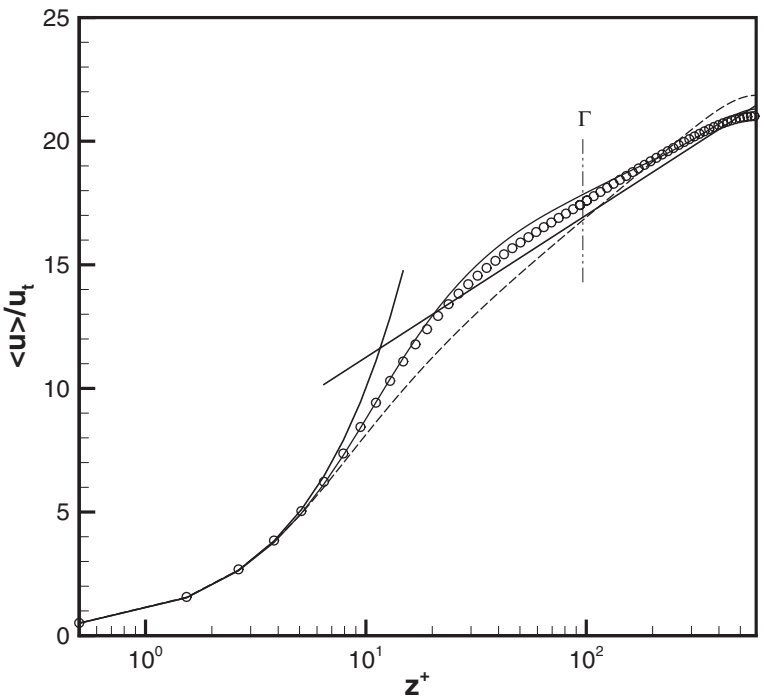

Figure 4. Mean velocity profiles at $Re_\tau = 590$: A1L: solid line; A1R: dashed line; A3: circle.

numerical method and the present grid resolution. The agreement between classical LES and the hybrid RANS/LES computations on the resolved Reynolds stresses is very good. The observed differences occurring near the interface are localized in a 4–5 point wide layer near the interface, and they are seen to not pollute the rest of the computation. The fluctuations observed in the RANS region are due to the unsteady character of the 1D RANS computation in that subdomain.

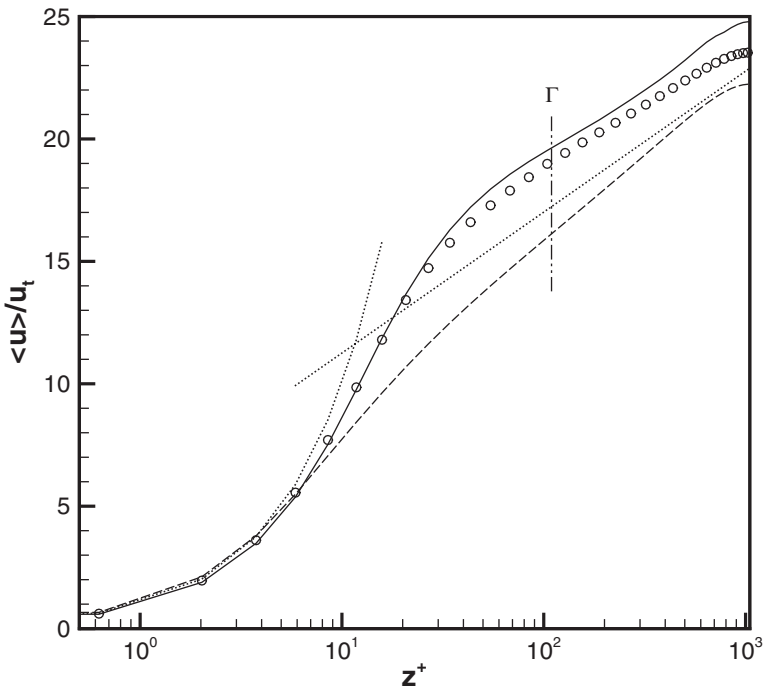

Figure 5. Mean velocity profiles at $Re_\tau = 1050$: B1L: solid line; B1R: dashed line; B3: circle; theoretical profiles: dotted line.

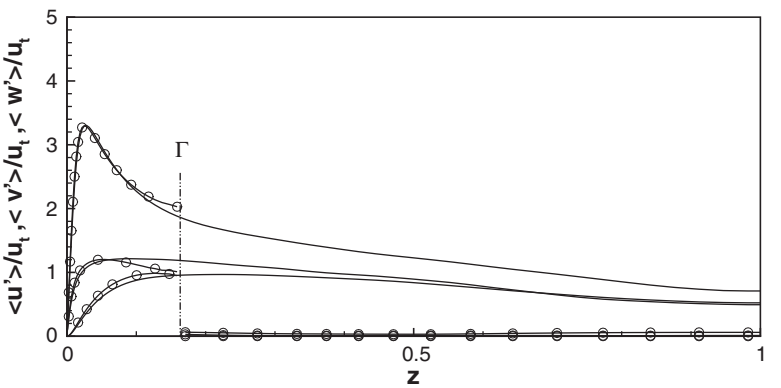

Figure 6. Streamwise, spanwise and wall-normal *rms* velocity fluctuations normalized with the skin friction at $Re_\tau = 590$: A1L: solid line; A3: line and circle.

The effect of the enrichment procedure is seen in Figure 8, where one-dimensional energy spectra near the interface are shown, and compared with those obtained in classical monodomain LES and hybrid RANS/LES without enrichment. The agreement obtained when using the enrichment procedure at the RANS/LES interface is very satisfactory, giving a new

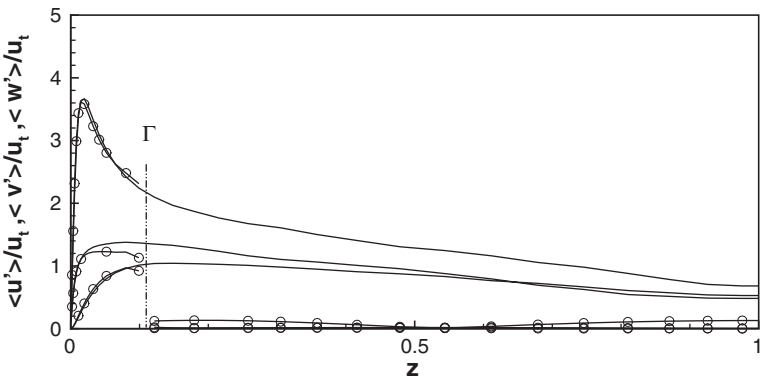

Figure 7. Streamwise, spanwise and wall-normal *rms* velocity fluctuations normalized with the skin friction at $Re_\tau = 1050$: B1L: solid line; B3: line-circle.

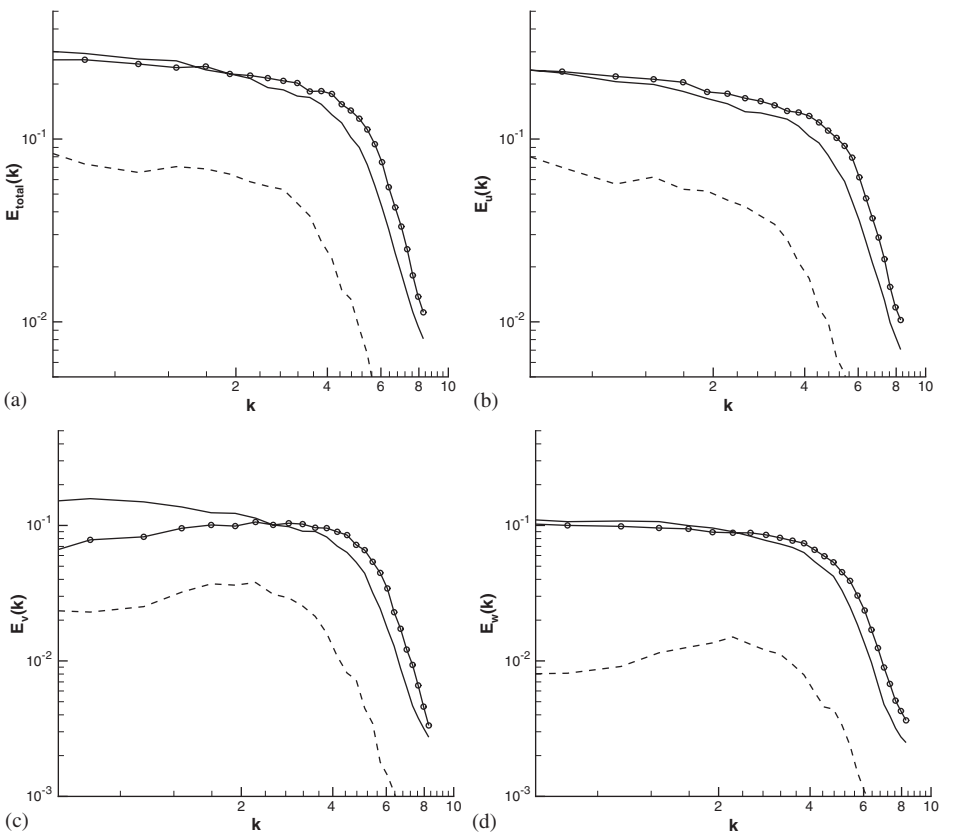

Figure 8. One-dimensional energy spectra close to the interface in the LES domain at $Re_\tau = 590$ (plane $z^+ = 95$): E_{total} (a), E_u (b), E_v (c), E_{w} (d). A1: solid line, A3: line-symbol, A3 ($C_{\text{extra}} = 0$): dashed line.

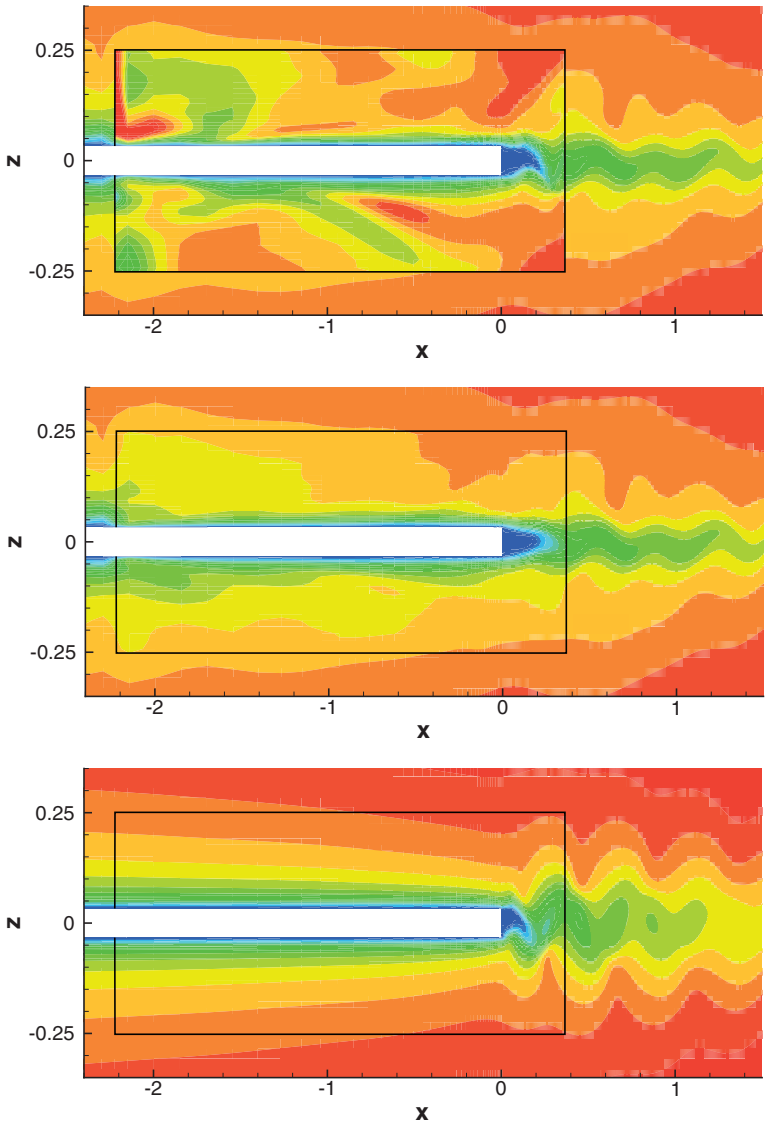

Plate 1. Streamwise velocity: (Top) RANS/LES approach; (middle) RANS/LES approach (spanwise-averaged value); (bottom) RANS calculation.

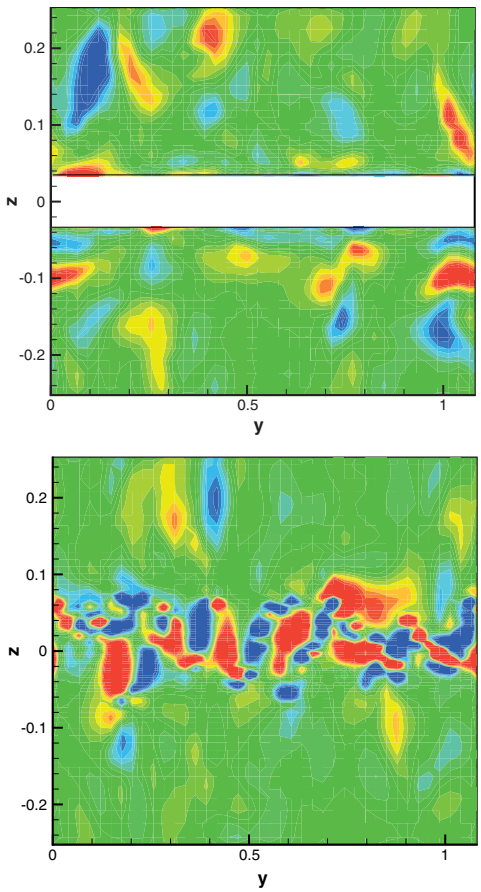

Plate 2. Instantaneous streamwise vorticity component: upstream trailing edge at $X/H = -4$ (top), in the wake at $X/H = +4$ (bottom).

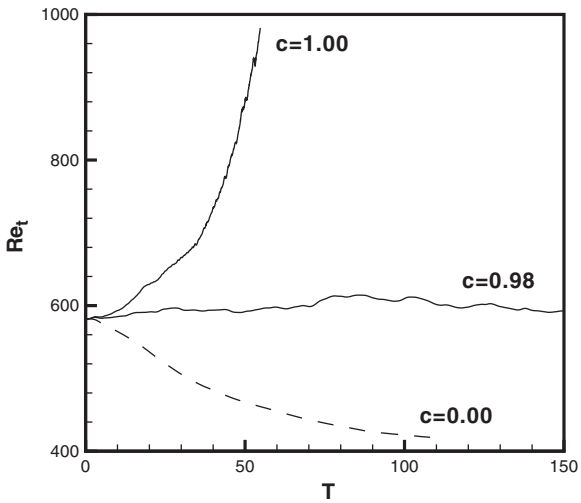

Figure 9. Effect of the enrichment procedure on the evolution of the friction Reynolds number (case A3).

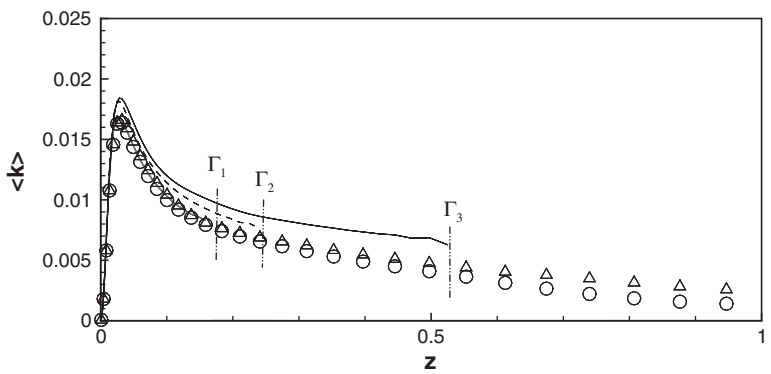

Figure 10. Resolved turbulent kinetic energy at $Re_\tau = 590$. A1L: circle; A3: solid line; A3+: dashed line; A3++: dotted line; A2: triangle.

validation of the method. Moreover, it is worth noting that without enrichment, as encountered for energy level close to the interface, the friction Reynolds number decreases strongly (Figure 9). This demonstrates the necessity to proceed to such a reconstruction.

The sensitivity of the method to the position of the interface is then investigated. The resolved kinetic energy profiles obtained for three different positions at $Re_\tau = 590$ are presented in Figure 10. A good general agreement is obtained with classical LES. It is also observed that some differences appear in the centre of the channel, as the cut-off is moved toward the centreline of the channel. Careful tests have demonstrated that this is due to a less satisfactory behaviour of the 1D RANS computation in the central subdomain, which is due to the fact that both its extent and its resolution are diminishing, yielding stronger fluctuation levels. But,

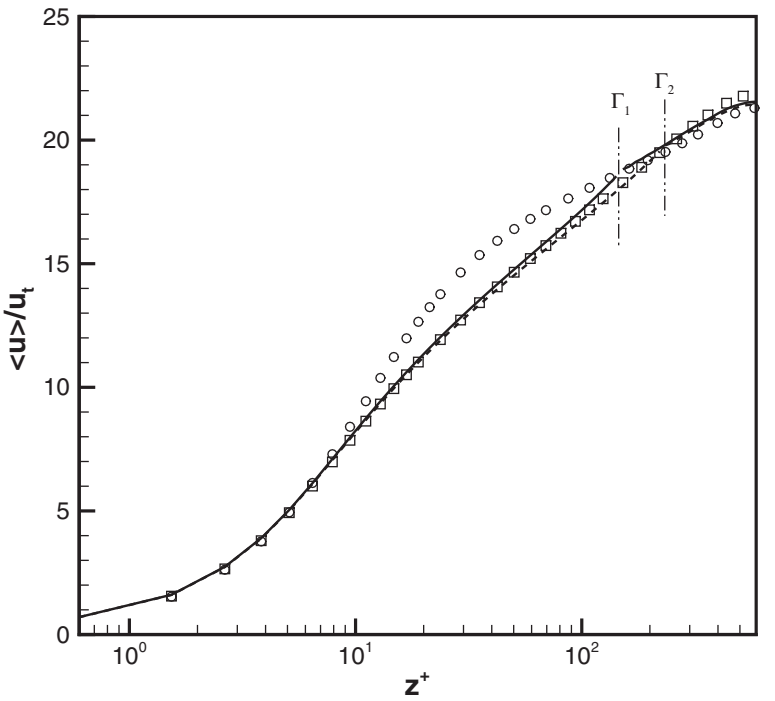

Figure 11. Mean velocity profiles: A3RLR: solid line; A3RLR+: dashed line; A1L: circle; A1R: square.

in all the cases, the RANS/LES coupling procedure remains efficient. A proof is the very good agreement between the classical LES computation and the A2 case, in which one-half of the channel is computed with LES, while the other part is computed by RANS.

6.3. Near-wall RANS treatment

We now present the results obtained when using the RANS approach for the near-wall region. Two cases have been considered, which correspond to different position of the interface (all computational parameters are given in Table II).

Computed mean velocity profiles are compared to classical LES and RANS computations in Figure 11. The observed perfect agreement between RANS and hybrid computations (in the RANS subdomains) shows that the near-wall behaviour in the hybrid computation is governed by the RANS model, and seems to be insensitive to the coupling procedure. In the LES subdomain, a very good agreement is recovered with all the other computations, demonstrating the efficiency of the interface condition.

Resolved Reynolds stresses are compared to results of usual LES in Figure 12. A very good agreement is obtained in the case where the interface is located at $z^+ = 150$, while more pronounced discrepancies near the interface are observed in the second case ($z^+ = 225$). This is explained by two facts: (i) in the second case the mesh size near the interface is greater, yielding higher extrapolation error in the ghost cells and, (ii) the mesh size near the interface being larger, it does not allow a very accurate description of turbulent fluctuation

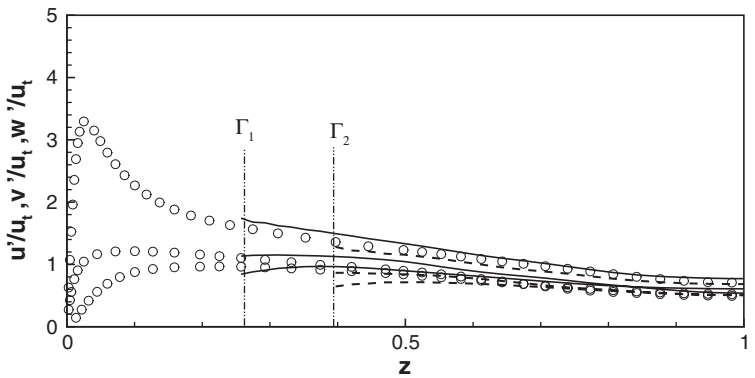

Figure 12. Streamwise, spanwise and wall-normal *rms* velocity fluctuations normalized with the skin friction at $Re_\tau = 590$: A3RLR: solid line; A3RLR+: dashed line; A1L: circle.

in this region, reducing the efficiency of the coupling procedure. But it is worth noting that, even in the second case, the results are at least as good as those obtained by other authors with other hybrid RANS/LES procedures. Two interesting remarks are that (i) no spurious boundary layer develops at the interface, as it is sometimes seen with wall stress models and (ii) turbulent fluctuations are maintained in the core of the channel, despite the near-wall production events are not captured in the LES regions. In both cases, the reconstruction of turbulent fluctuations at the interface seems to be a key point of the present method [26].

7. APPLICATION TO THE FLOW PAST A BLUNT TRAILING EDGE

7.1. Domain decomposition and computational parameters

The last configuration is the subsonic flow around a flat plate with a blunt trailing edge. The purpose is here to predict accurately the vortex shedding near the trailing edge in a very small subdomain, which is representative of the location of acoustic sources in that flow (see Reference [27] for a classical LES treatment of this flow). This configuration involves high-normal velocity inflow interface for the LES subdomain, and will then make it possible to analyse the proposed coupling procedure.

The Reynolds number $Re_\infty = U_\infty L/\nu$, where U_∞ is the external reference velocity and L the length of the plate, is taken equal to 2.10^6. The reference Mach number is equal to 0.5. The thickness H of the plate is taken equal to $L/2300$, which is representative of what is encountered on realistic wing profiles. The corresponding values in wall units are $L^+ = 66\,000$ and $H^+ = 29$, based on the friction velocity computed just near the separation point with a RANS computation (the friction Reynolds number at this point is equal to 436).

The subdomain decompositions is displayed on Figure 13. A view of the mesh near the trailing edge is presented in Figure 14. Geometrical parameters associated to this case (expressed in wall units) are summarized in Table IV. The distance between the trailing edge and the upstream (respectively, downstream) inflow interface of the LES subdomains in the streamwise (x) direction is referred to as $X2^+$ ($X3^+$). The distance of the horizontal LES

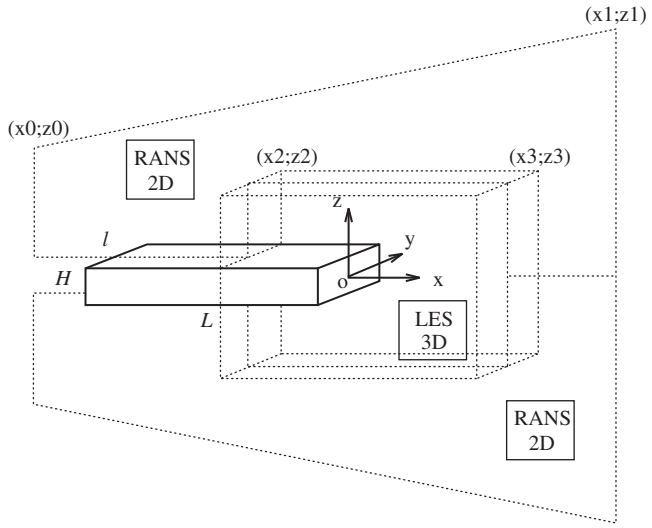

Figure 13. Blunted trailing-edge configuration.

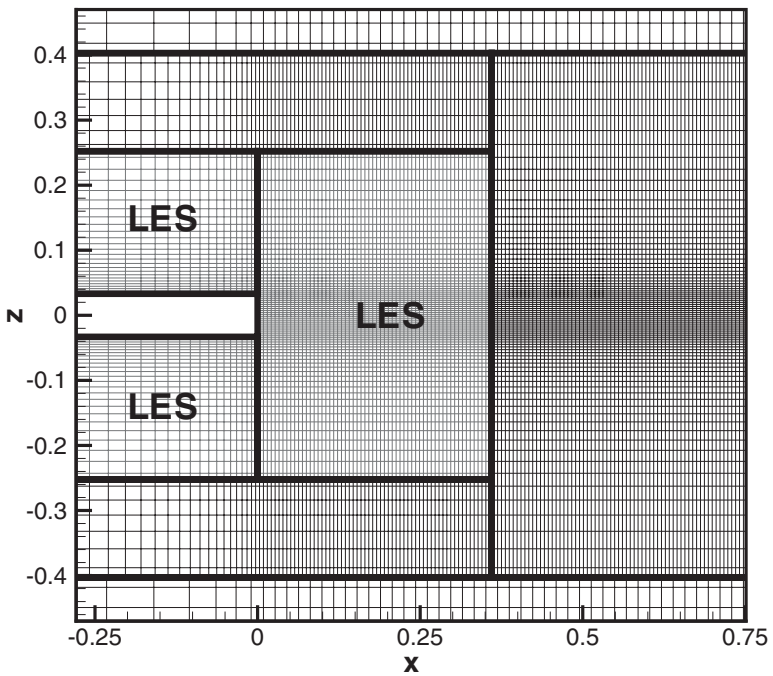

Figure 14. View of the mesh near the trailing edge.

Table IV. Geometrical parameters for the LES-subdomains definition for blunt trailing-edge computations.

$X2^+$	$X3^+$	$Z2^+\|_w$	L_y^+	Δx^+	Δy^+	$\Delta z^+\|_w$
−968	156	95	327.7	2.6–64	11.7	1.3

subdomain to the flat plate is noted $Z2^+|_w$. The spanwise extent of the LES subdomains is L_y^+ (it is recalled that the RANS subdomain are 2D and have a null spanwise extent). The size of the first mesh near the separation point is also given. For the LES subdomains, a uniform mesh spacing is used in the wake region, while a stretched grid is employed upstream the trailing edge. The mesh is stretched in the wall-normal direction, and uniform in the spanwise direction.

The total number of grid points is nearly equal to 360 000, the LES part corresponding approximatively to 270 000 points. The total number of subdomains is 14 (10 RANS subdomains, 3 LES subdomains and one additional domain for the independant channel plane flow simulation), leading to the definition of approximatively 100 interfaces, with 7 interfaces corresponding to RANS/LES coupling.

7.2. High-normal velocity inflow interface treatment

As said in Section 4.2, a specific way to reconstruct w_{12} at the LES subdomain interface located at $x = X2$ has been defined, which is now described.

The reconstruction relies on the use of a secondary LES of plane channel flow, in order to have a realistic fluctuation profile. The instantaneous fluctuations around the mean profile in the channel flow at a given streamwise position are extracted, rescaled in wall units, and used as the w_{12} field at the RANS/LES interface. This procedure was used at each time step of the blunted flat-plate flow simulation.

7.3. Results

Some instantaneous flow fields are displayed in Plates 1 and 2. Plate 1 presents three different instantaneous streamwise velocity components in a $(x–z)$ plane: the velocity extracted from a single plane from the LES subdomains and the velocity in the RANS subdomains, the spanwise-averaged velocity in the LES subdomains and the velocity in the RANS subdomains, and the velocity obtained carrying out a 2D unsteady RANS computation. Plate 2 displays instantaneous views of the streamwise vorticity component in two $(y–z)$ planes in the LES subdomains. The first one is located upstream the trailing edge, while the second is located in the wake region.

A fully 3D behaviour in the LES subdomains is observed, thanks to the use of the enrichment procedure at the inflow interface of the LES region. Classical structures associated to near-wall turbulence are present. An interesting feature of the simulation is the discontinuity of the velocity field at the RANS/LES interface. That discontinuity is seen to vanish when the spanwise-averaged velocity field is considered in the LES subdomain instead of the 3D field, in agreement with the fact that this direction is assumed to be an homogeneous direction for this flow.

The vortex shedding mechanism is characterized by the main value of the Strouhal number St. The computed values are $St = 0.55$ and 0.59 for the 2D RANS and the hybrid RANS/LES computations, respectively, yielding to a good agreement. It is worth noting this value is sensitive to the enrichment procedure: numerical simulation without enrichment at the RANS/LES interface yields $St = 0.85$, because turbulence effect are missing.

In a general way, no deleterious effects (such as spurious wiggles or reflecting waves from outflow RANS/LES interface) are detected. Thus, at least on a qualitative point of view, these results demonstrate the ability of the multi-domain/multi-resolution method to deal with problems on complex geometries.

8. CONCLUSIONS

A new zonal RANS/LES computational technique is proposed. It is based on the use of a subdomain decomposition, each domain being treated using one of these two approaches. Theoretical analysis reveals that the solution is discontinuous at the RANS/LES interface, and that even the dimension of the solution can vary. As a consequence, the RANS/LES coupling strategy appears as a generalized multi-domain problem. The proposed treatment is based on the definition of an interface variable, which is extrapolated from the LES subdomain or extracted from an auxiliary computation, depending on the type of interface.

The proposed procedure was successfully assessed on the plane channel configuration and on the flow past a blunt trailing edge. Both mean velocity and resolved Reynolds stresses profiles are recovered, demonstrating the efficiency of the method.

For interfaces referred to as low-normal velocity interfaces, the extrapolation of the w_{12} field from the LES subdomain seems to be adequate. For high-normal velocity interfaces, good results were obtained using fluctuations extracted from an auxiliary LES.

REFERENCES

1. Sagaut P. *Large-Eddy Simulation for Incompressible Flows*. Springer: Berlin, 2002.
2. Spalart PR, Jou WH, Strelets M, Allmaras SR. Comments on the feasibility of LES for wings, and on hybrid RANS/LES approach. *Proceedings of the 1st AFOSR International Conference on DNS/LES*, Ruston, LA, August 4–8, 1997.
3. Speziale CG. Turbulence modeling for time-dependent RANS and VLES: a review. *American Institute of Aeronautics and Astronautics Journal* 1998; **36**(2):173–184.
4. Nikitin NV, Nicoud F, Wasistho B, Squires KD, Spalart PR. An approach to wall modelling in large-eddy simulation. *Physics of Fluids* 2000; **12**(7):1629–1632.
5. Quéméré P, Sagaut P, Couaillier V. A new multi-domain/multi-resolution method for large-eddy simulation. *International Journal for Numerical Methods in Fluids* 2001; **36**:391–416.
6. Ghosal S, Moin P. The basic equations for the large-eddy simulation of turbulent flows in complex geometry. *Journal of Computational Physics* 1995; **118**:24–37.
7. Vasilyev O, Lund TS, Moin P. A general class of commutative filters for LES in complex geometries. *Journal of Computational Physics* 1998; **146**:82–104.
8. Lenormand E, Sagaut P, Loc TP. Large-Eddy simulation of compressible channel flow at moderate Reynolds number. *International Journal for Numerical Methods in Fluids* 2000; **32**:369–406.
9. Lenormand E, Sagaut P, Loc TP, Comte P. Subgrid-scale models for large-Eddy simulation of compressible wall bounded flows. *American Institute of Aeronautics and Astronautics Journal* 2000; **38**(8):1340–1350.
10. Vreman B, Geurts B, Kuerten H. A priori tests of large-eddy simulation of compressible plane mixing layer. *Journal of Engineering Mathematics* 1995; **29**:299–327.
11. Sagaut P, Grohens R. Discrete filters for large-eddy simulation. *International Journal for Numerical Methods in Fluids* 1999; **31**:1195–1220.

12. Jones WP, Launder BE. The prediction of laminarization with a two-equation model of turbulence. *International Journal of Heat and Mass Transfer* 1972; **15**:301–314 .
13. Labourasse E, Sagaut P. Reconstruction of turbulent fluctuations using a hybrid RANS/LES approach. *Journal of Computational Physics*, 2002 at press.
14. Carati D, Rogers MM. Ensemble-averaged LES of time-evolving plane wake. *Proceedings of the Summer Program—Center for Turbulence Research* 1998; 325–336.
15. Carati D, Wray A, Cabot W. Ensemble-averaged dynamic modeling. *Proceedings of the Summer Program—Center for Turbulence Research* 1996; 237–248
16. Nicoud F, Winckelmans G, Carati D, Bagget J, Cabot W. Boundary conditions for LES away from the wall. *Proceedings of the Summer Program—Center for Turbulence Research* 1998; 413–422.
17. Chung YM, Sung HJ. Comparative study of inflow conditions for spatially evolving simulation. *American Institute of Aeronautics and Astronautics Journal* 1997; **35**(2):269–274.
18. Lund TS, Wu X, Squires KD. On the generation of turbulent inflow conditions for boundary-layer simulations. *Journal of Computational Physics* 1998; **140**:233–258.
19. Ducros F, Sagaut P, Quéméré P. On the use of relaxation procedure for localized dynamic models. *Physics of Fluids* 2000; **12**(12):3297–3300.
20. Terracol M, Sagaut P, Basdevant C. A multilevel algorithm for large-eddy simulation of turbulent compressible flows. *Journal of Computational Physics* 2001; **167**(2):1–36.
21. Balaras E, Benocci C, Piomelli U. Two-layer approximate boundary conditions for large-eddy simulations. *American Institute of Aeronautics and Astronautics Journal* 1996; **34**(6):1111–1119.
22. Cabot W. Near-wall models in large-eddy simulations of flow behind a backward-facing step. *Annual Research Briefs—Center for Turbulence Research* 1996; 199–210.
23. Cabot W. Large-eddy simulations with wall models. *Annual Research Briefs—Center for Turbulence Research* 1995; 41–49.
24. Jimenez J, Pinelli A. The autonomous cycle of near-wall turbulence. *Journal of Fluid Mechanics* 1999; **389**: 335–359.
25. Jimenez J, Simens MP. Low-dimensional dynamics of a turbulent wall flow. *Journal of Fluid Mechanics* 2001; **435**:81–91.
26. Nicoud F, Bagget JS, Moin P, Cabot W. Large-eddy simulation wall-modeling based on sub-optimal control theory and linear stochastic estimation. *Physics of Fluids* 2001; **13**(10):2968–2984.
27. Manoha E, Troff B, Sagaut P. Trailing-edge noise prediction using large-eddy simulation and acoustic analogy. *American Institute of Aeronautics and Astronautics Journal* 2000; **38**(4):575–583.

